A&A 482, 529–534 (2008)
DOI: 10.1051/0004-6361:20078796

Astronomy & Astrophysics

Millimeter observations of planetary nebulae

A contribution to the Planck pre-launch catalogue

G. Umana[1], P. Leto[1,2], C. Trigilio[1], C. S. Buemi[1], P. Manzitto[3], S. Toscano[3], S. Dolei[3], and L. Cerrigone[3,4]

[1] INAF – Osservatorio Astrofisico di Catania, via S. Sofia 78, 95123 Catania, Italy
e-mail: Grazia.Umana@oact.inaf.it
[2] INAF Istituto di Radioastronomia, Sezione di Noto, C.P. 161, Noto (SR), Italy
[3] Universitá di Catania, Dipartimento di Fisica e Astronomia, via S. Sofia 78, 95123 Catania, Italy
[4] Harvard-Smithsonian Center for Astrophysics, Cambridge, MA 02138, USA

Received 5 October 2007 / Accepted 18 January 2008

ABSTRACT

Aims. We present 43 GHz (7 mm) observations of a sample of radio-bright Planetary nebulae aimed to obtain, together with far-IR measurements (IRAS), reliable estimates of the fluxes emitted in the millimetre and sub-millimetre band, and, therefore, to test their detectability by the forthcoming ESA PLANCK mission. This spectral range, even though very important to constrain the physics of circumstellar environments, is still far from being completely exploited.
Methods. The new millimetre 43 GHz observations were obtained by using the 32 m INAF-IRA Noto Radiotelescope. To estimate the millimetre and sub-millimetre fluxes, we extrapolated and summed the ionized gas (free-free radio emission) and dust (thermal emission) contributions in this frequency range. By comparison of the derived flux densities to the predicted sensitivity we investigate the possible detection of such source for all the channels of PLANCK
Results. We conclude that almost 80% of our sample will be detected by PLANCK, with a higher detection rate in the higher frequency channels, where there is a good combination of brighter intrinsic flux from the sources and reduced extended Galactic foregrounds contamination despite poorer instrumental sensitivity. From the new 43 GHz, combined with single-dish 5 GHz observations from the literature, we derive radio spectral indexes, which are consistent with optically thin free-free nebula. This result indicates that the high frequency radio spectrum of our sample sources is dominated by thermal free-free, and other emissions, if present, are negligible.

Key words. ISM: planetary nebulae: general – radio continuum: general – radio continuum: stars

1. Introduction

The PLANCK ESA mission will provide nearly full sky maps over a wide range of frequencies, from 30 to 900 GHz. Therefore, even if designed for cosmological studies, the mission will have a profund impact on fundamental physics and Galactic and extragalactic astrophysics. Planck will be sensitive to the millimetre emission from dusty envelopes of stars and we expect the dusty circumstellar envelopes, that characterize the later stages of stellar evolution, to be source of a foreground contamination. When a low or intermediate mass star is approaching the end of its evolution, it goes through a period of heavy mass-loss known as the Asymptotic Giant Branch (AGB) phase. The ejected envelopes are partially condensed in dust grains and completely obscure the central star. Immediately after the AGB evolutionary phase, the mass-loss stops and the stars may become optically visible as the dusty shells disperse (Proto Planetary Nebula, PPN phase). Eventually, once it reaches a temperature of $2{-}3 \times 10^4$ K, the central star starts to ionize the AGB shell and a Planetary Nebula will form. Dusty envelopes re-radiate the absorbed stellar light showing a clear signature in the far-infrared spectrum, i.e. an IR excess with peculiar IRAS colours. In addition to that, PNe show a radio continuum due to free-free emission from the fraction of the CSE ionized by the central star.

From a feasibility study, Umana et al. (2006) concluded that a sizable (≈300) sample of AGB and post-AGB stars would be detected during the mission and derived estimates for the expected flux densities at various Planck channels. However, the simulations carried out by Umana et al. (2006) on a subsample of PNe rely only on the 1.4 GHz NRAO VLA Sky Survey (NVSS) fluxes, extrapolated to the Planck frequencies. This leads to underestimation of the contribution due to free-free emission as, at this frequency, PNe are often optically thick (Siódmiak & Tylenda 2001; Luo et al. 2005).

PNe are among the brightest Galactic radio sources. Some of them could also reach a flux density of Jy level. More than 800 have been detected at least at one frequency and for 200 morphological and spectral information (between 1.4 and 22 GHz) were obtained. Most of the higher frequency (22 GHz) data were obtained with interferometers (i.e. VLA) while very few single-dish, high frequency measurements are available.

In this paper we present new 43 GHz, single-dish observations using the 32 m INAF-IRA Radiotelescope at Noto of a sample of PNe, which are potential foregrounds for PLANCK. The main goal of this project is to obtain reliable estimates of the flux density expected in PLANCK channels, by building and modeling their spectral energy distribution (SED). This in turn will contribute to the compilation of the PLANCK pre-launch catalogue. 43 GHz is one of the observing channels of the forthcoming PLANCK mission. Therefore, at this frequency band,

Table 1. The selected sample.

IAU Name PN G	Other Name	RA (J2000) [h m s]	Dec (J2000) [° ′ ″]	IAU Name PN G	Other Name	RA (J2000) [h m s]	Dec (J2000) [° ′ ″]
000.3 + 12.2	IC 4634	17 01 33.6	−21 49 33.1	093.4 + 05.4	NGC 7008	21 00 32.7	+54 32 39.4
002.4 + 05.8	NGC 6369	17 29 20.5	−23 45 35.0	093.5 + 01.4	PN M 1-78	21 20 44.8	+51 53 27.5
003.1 + 02.9	PN Hb 4	17 41 52.8	−24 42 09.3	096.4 + 29.9	NGC 6543	17 58 33.4	+66 37 58.8
006.7 − 02.2	PN M 1-41	18 09 30.6	−24 12 28.7	097.5 + 03.1	PN A66 77	21 32 10.2	+55 52 43.2
007.2 + 01.8	PN HB 6	17 55 07.0	−21 44 41.0	106.5 − 17.6	NGC 7662	23 25 53.9	+42 32 04.7
008.0 + 03.9	NGC 6445	17 49 15.0	−20 00 33.7	107.8 + 02.3	NGC 7354	22 40 19.9	+61 17 08.0
008.3 − 01.1	PN M 1-40	18 08 26.0	−22 16 53.4	120.0 + 09.8	NGC 40	00 13 01.0	+72 31 19.6
009.4 − 05.0	NGC 6629	18 25 42.5	−23 12 11.3	130.9 − 10.5	NGC 650-51	01 42 19.7	+51 34 31.7
009.6 + 14.8	NGC 6309	17 14 04.3	−12 54 37.2	138.8 + 02.8	IC 289	03 10 19.3	+61 19 00.4
010.1 + 00.7	NGC 6537	18 05 13.1	−19 50 34.4	144.5 + 06.5	NGC 1501	04 06 59.3	+60 55 14.7
010.8 − 01.8	NGC 6578	18 16 16.5	−20 27 03.4	165.5 − 15.2	NGC 1514	04 09 16.9	+30 46 32.0
011.7 − 00.6	NGC 6567	18 13 45.2	−19 04 35.6	166.1 + 10.4	IC 2149	05 56 23.9	+46 06 17.4
020.9 − 01.1	PN M 1-51	18 33 29.0	−11 07 26.3	173.7 + 02.7	PP 40	05 40 52.7	+35 42 18.6
025.8 − 17.9	NGC 6818	19 43 57.8	−14 09 11.8	194.2 + 02.5	J 900	06 25 57.3	+17 47 27.6
027.7 + 00.7	PN M 2-45	18 39 21.9	−04 19 52.6	197.8 + 17.3	NGC 2392	07 29 10.8	+20 54 41.6
033.8 − 02.6	NGC 6741	19 02 37.0	−00 26 57.2	206.4 − 40.5	NGC 1535	04 14 15.8	−12 44 22.3
034.6 + 11.8	NGC 6572	18 12 06.3	+06 51 12.4	215.2 − 24.2	IC 418	05 27 28.2	−12 41 50.2
035.1 − 00.7	PN Ap 2-1	18 58 10.5	+01 36 57.5	221.3 − 12.3	IC 2165	06 21 42.8	−12 59 13.9
037.7 − 34.5	NGC 7009	21 04 10.8	−11 21 48.5	234.8 + 02.4	NGC 2440	07 41 55.4	−18 12 30.5
039.8 + 02.1	PN K 3-17	18 56 18.2	+07 07 26.2	254.6 + 00.2	NGC 2579	08 20 54.1	−36 13 00.0
041.8 − 02.9	NGC 6781	19 18 28.1	+06 32 20.0	258.1 − 00.3	Hen 2-9	08 28 28.0	−39 23 39.4
043.1 + 37.7	NGC 6210	16 44 29.5	+23 47 59.9	259.1 + 00.9	Hen 2-11	08 37 08.1	−39 25 04.9
045.7 − 04.5	NGC 6804	19 31 35.1	+09 13 30.2	261.0 + 32.0	NGC 3242	10 24 46.1	−18 38 32.3
050.1 + 03.3	PN M 1-67	19 11 31.1	+16 51 32.0	294.1 + 43.6	NGC 4361	12 24 30.8	−18 47 04.0
054.1 − 12.1	NGC 6891	20 15 08.9	+12 42 15.4	342.1 + 10.8	NGC 6072	16 12 58.4	−36 13 46.6
063.1 + 13.9	NGC 6720	18 53 35.1	+33 01 45.1	349.5 + 01.0	NGC 6302	17 13 44.5	−37 06 11.6
064.7 + 05.0	BD+30 3639	19 34 45.2	+30 30 59.2	352.6 + 00.1	PN H 1-12	17 26 24.3	−35 01 41.8
082.1 + 07.0	NGC 6884	20 10 23.7	+46 27 40.0	352.8 − 00.2	PN H 1-13	17 28 27.7	−35 07 30.4
083.5 + 12.7	NGC 6826	19 44 48.2	+50 31 31.3	358.5 + 02.6	PN HDW 8	17 31 47.3	−28 42 03.5
086.5 − 08.8	PN Hu 1-2	21 33 08.2	+39 38 08.3	358.5 + 05.4	PN M 3-39	17 21 11.5	−27 11 37.0
089.0 + 00.3	NGC 7026	21 06 18.7	+47 51 07.5	359.3 − 00.9	Pn HB 5	17 47 56.3	−29 59 40.6

we would obtain a direct measurement of the expected flux and not an extrapolation.

As an added value, the present work provides the first sizeable dataset of 43 GHz measurements of PNe that constitute strong constraints to the observed SEDs in the very important spectral region where free-free emission and thermal dust emission may overlap. While interferometric high frequency observations provide us with detailed morphological information they quite often fail to entirely recover the extended emission. This eventually leads to underestimation of the total radio flux density. This problem is overcame by single-dish observations. The knowledge of the SEDs in the radio-millimetre spectral range is a crucial step for the study of the physics of dusty envelopes around PN. A correct evaluation of the free-free contribution, up to the millimetre range, when combined with information provided by far-IR observations, would allow us to determine the presence of an excess due to the existence of a cold dust component**(s)** (Gee et al. 1984; Hoare et al. 1992; Kemper et al. 2002) or of alternative emission mechanisms (Casassus et al. 2007). Since PNe and their progenitors are believed to be among the major sources of recycled interstellar matter, determining the properties of the dust ejected in the ISM is very important to the study of the Galaxy evolution in general.

2. The 43 GHz Noto survey

2.1. sample selection

Our sample has been selected mainly from Condon & Kaplan (1998), who performed a cross-correlation between the Strasbourg-ESO Catalogue of Galactic Planetary Nebulae (Cat. ⟨V/84⟩, Acker et al. 1992) and the 1.4 GHz NRAO VLA Sky Survey. Among these sources we selected only those whose flux densities at 1.4 GHz (NVSS) is higher than 100 mJy, for a total of 64 PNe. In the conservative hypothesis of optically thin nebula at 1.4 GHz, a cut-off at 100 mJy guarantees a 43 GHz flux density easily detectable with the Noto Radiotelescope. This estimated 43 GHz flux density will be a lower limit in the case of optically thick nebula at 1.4 GHz. We also considered Condon et al. (1999) who selected infrared PNs in NVSS by a cross-correlation between NVSS and a sample from IRAS PSC on the basis of infrared colours characteristic of PNe. Only 3 of the 122 infrared PNs candidate have $S_{1.4\ \mathrm{GHz}} \geq 100$ mJy, yielding a final sample of 67 objects.

To avoid problems due to possible contamination in the Noto beam ($HPBW = 54''$), for each source of the sample, we have extract from NVSS a $25' \times 25'$ field, centred at the position of the target. Sources that show a very extended ($\geq 2'$) emission or that are located in very high confusion region have been rejected. This reduces our sample to 62 objects. The list of the selected targets, with names and positions, is reported in Table 1.

2.2. Observations and results

In the last few years the INAF-IRA 32 m Noto radiotelescope has undergone a series of structural improvements which have remarkably increased its capabilities as a single dish instrument.

Table 2. Results. The columns are as following: source name (1); Noto measured flux density and its associated error (2 and 3); Gaussian source angular dimension as from NVSS (4); actual diameter of the source (5); total flux density corrected as explained in the text (6).

IAU Name PN G	S_{43} [mJy]	σ_{43} [mJy]	$\theta_{1.4}$ [″]	Θ [″]	$S_{43}^{(I)}$ [mJy]	Ref.*	IAU Name PN G	S_{43} [mJy]	σ_{43} [mJy]	$\theta_{1.4}$ [″]	Θ [″]	$S_{43}^{(c)}$ [mJy]	Ref.*
000.3+12.2	<180	60	10	–	–	4, 7	093.4+05.4	<240	80	49	72	–	2, 1
002.4+05.8	1330	110	21	33	1530	4, 7	093.5+01.4	560	35	15	23	600	2, 1
003.1+02.9	100	20	12	–	100	4, 7	096.4+29.9	400	70	12	–	420	2, 1
006.7-02.2	300	90	21	33	350		097.5+03.1	230	25	33	51	320	2, 1
007.2+01.8	310	50	11	–	320	4, 7	106.5-17.6	610	40	12	–	640	2, 1
008.0+03.9	180	20	35	53	250	4, 6	107.8+02.3	280	25	16	26	310	2, 1
008.3-01.1	90	20	10	–	90	4, 7	120.0+09.8	420	70	28	43	530	2, 1
009.4-05.0	130	30	13	20	140	4, 7	130.9-10.5	140	40	59	85	310	2, 1
009.6+14.8	270	60	14	23	290	4, 7	138.8+02.8	<150	50	23	36	–	2, 1
010.1+00.7	400	60	12	–	420	4, 5, 7	144.5+06.5	215	30	35	53	300	2, 1
010.8-01.8	130	20	12	–	140	4, 7	165.5-15.2	220	30	94	129	890	2, 1
011.7-00.6	<150	50	9	–	–	4, 7	166.1+10.4	100	30	9	–	100	2, 1
020.9-01.1	420	90	14	21	450	4	173.7+02.7	260	20	12	–	270	1
025.8-17.9	270	30	15	23	290	4, 7	194.2+02.5	90	20	0	–	90	2, 1, 7
027.7+00.7	110	20	0	–	110	3, 6	197.8+17.3	240	50	22	35	280	2, 1, 7
033.8-02.6	290	50	15	23	310	1, 7	206.4-40.5	160	20	21	32	180	4, 7
034.6+11.8	1220	100	12	–	1280	2, 1, 7	215.2-24.2	1100	100	0	–	1100	4, 7
035.1-00.7	170	20	13	21	180	2, 1	221.3-12.3	350	50	11	–	360	4, 7
037.7-34.5	375	40	15	24	400	4, 7	234.8+02.4	350	20	17	26	380	4, 7
039.8+02.1	240	20	0	–	240	2, 1	254.6+00.2	1770	290	41	62	2800	5
041.8-02.9	230	20	78	109	710	2, 1, 7	258.1-00.3	180	40	5	–	180	8, 7
043.1+37.7	230	30	11	–	240	2, 1, 7	259.1+00.9	270	60	42	63	430	8
045.7-04.5	140	20	25	40	170	2, 3, 1	261.0+32.0	290	30	20	31	330	4, 7
050.1+03.3	140	30	41	62	220	2, 1, 7	294.1+43.6	130	20	47	70	230	4, 7
054.1-12.1	130	40	9	–	130	2, 1, 7	342.1+10.8	<210	70	33	50	–	7
063.1+13.9	255	75	48	71	460	2, 1	349.5+01.0	2150	220	15	23	2310	8, 5, 7
064.7+05.0	565	20	11	–	590	2, 1	352.6+00.1	815	125	10	–	840	5
082.1+07.0	250	50	11	–	260	2, 1	352.8-00.2	420	50	15	23	450	5
083.5+12.7	320	40	16	25	350	2, 1	358.5+02.6	<120	40	21	33	–	4, 6
086.5-08.8	<120	40	10	–	–	2, 1	358.5+05.4	380	40	0	–	380	4, 6
089.0+00.3	220	30	12	–	230	2, 1	359.3-00.9	290	70	0	–	290	5, 7

* References for 5 GHz measurements: 1) Becker et al. (1991); 2) Gregory et al. (1996); 3) Griffith et al. (1995); 4) Griffith et al. (1994); 5) Haynes et al. (1979); 6) Milne (1979); 7) Milne (1975); 8) Wright et al. (1994).

In particular, the installation of an active surface allows it to operate with good performance at high frequencies.

The observations reported in this paper were carried out in different epochs, between 2005 and 2006. The 43 GHz superheterodyne receiver is a cooled double polarization receiver, with a typical zenith system temperature ($T_{\rm sys}$), in both channels, of the order of 80−100 K, depending on the weather conditions. The gain ranges from 0.05 to 0.1 K/Jy (Leto et al. 2006), depending on elevation, and this determines a zenith System Equivalent Flux Density (SEFD) of 1600−2000 Jy. The observations were performed with a 400 MHz instantaneous band.

All the sources of our sample were observed with the on the fly (OTF) scan technique, which consists of driving the beam of the telescope across the source in RA direction. The typical scan duration was of the order of 20 s, short enough to remain close to the white noise regime of the radiometer. In order to achieve a good signal to noise ratio, each source was observed many times, for a total integration time of 30 min. Multiple OTF scans were then added reaching a typical rms of 2−3 mK.

Daily gain curves were obtained and the flux scale was fixed by using NGC 7027 as the primary calibrator and 3C 286 as the secondary calibrator. The adopted flux densities for NGC 7027 and 3C 286 are respectively 5.07 and 1.86 Jy. The assumed flux densities are those reported by Ott et al. (1994); in the case of NGC 7027 the measure has been corrected for the observed decreament of 0.15 percent/year as reported by Perley et al. (2006).

We detected 55 out of the 62 observed objects, with a 89% detection rate. The results of such observations are reported in Table 2, where the 43 GHz measured flux density, or its 3σ upper limit, is listed (Col. 2). In the 4th and 10th columns of the same table we report the angular size at 1.4 GHz of each source ($\theta_{1.4}$), as derived from the analysis of the relative NVSS map, which has an angular resolution of 45″($\theta_{\rm NVSS}$). The source angular size has been derived as the geometrical mean of the minor and major axes obtained by fitting a two dimensional Gaussian at the source position in the map of the brightness distribution, and by performing a Gaussian deconvolution by means of the task JMFIT of the NRAO **A**stronomical **I**mage **P**rocessing **S**ystem (AIPS). In the case of partially resolved sources, this Gaussian angular diameter is related to the actual diameter of the source by a shape factor that accounts for the true structure of the source. Therefore, to compare the results from 1.4 GHz data with those obtained in the optical, we need to correct the Gaussian angular diameters following van Hoof (2000). This correction has been applied only for sources with $\theta_{1.4} \geq 1/4\theta_{\rm NVSS}$, assuming a uniform density model; the obtained values are reported in Table 2 (Θ). Such radio derived values are generally in good agreement with those given by Tylenda et al. (2003), derived

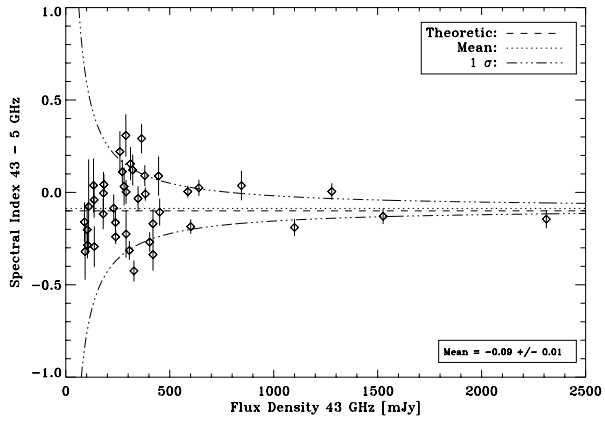

Fig. 1. Calculated 5–43 GHz spectral index as a function of flux at 43 GHz. As expected major dispersion is evident at lower fluxes.

from H_α images, with a few exceptions for PNe with very complex optical morphologies (i.e. Hb5 and M3-39) or in the case of NGC 6302, where the radio source is much smaller than the optical one (Gomez et al. 1989).

To take into account possible partial resolution of the source by the Noto beam, assuming that the source size at 43 GHz is the same as measured at 1.4 GHz, we corrected the measured flux density as

$$S^I_{43} = S_{43} \times \frac{\theta^2_{\rm Noto} + \theta^2_{1.4}}{\theta^2_{\rm Noto}}$$

where $\theta_{1.4}$ and $\theta_{\rm Noto}$ are the Gaussian diameter of the source at 1.4 GHz (reported in Table 2) and the width of the Noto radiotelescope beam ($HPBW = 54''$) respectively. Sources having an angular size greather than $25''$, comparable to the 43 GHz Noto beam ($HPBW$), have flux corrections that are significantly larger than the rms associated with the flux density. This means that they cannot be regarded as point-like. The resulting fluxes S^I_{43} are listed in Table 2.

3. The SEDs

3.1. The free-free contribution

As a first step in our analysis, we derived the spectral index α, ($S_\nu \propto \nu^\alpha$), by combining the fluxes measured at 43 GHz with the 5 GHz single dish measurements available from the literature. To prevent any error due to resolving out some of the flux density, we considered only the objects that have angular size, at 1.4 GHz ($\theta_{1.4\ \rm GHz}$), lower than $25''$. This reduces our sample of detected sources to 42 PNe that can be considered point-like with respect to the telescope beam at the observational frequency. Literature 5 GHz data are available only for 41 targets. The 5 GHz single dish measurements are from surveys performed by the NRAO Green Bank 91 m telescope, with a beamwidth ($HPBW$) ≈3.5′ (Gregory et al. 1996; Becker et al. 1991) and Parke s 64 m telescope with a beamwidth ≈4.5′ (Griffith et al. 1995, 1994; Wright et al. 1994; Haynes et al. 1979; Milne 1979; Milme & Aller 1975), as indicated in Table 2. For the sources observed in more than one survey, we used the average of the fluxes from the different measurements.

The spectral indices α, calculated between the two frequencies, are shown in Fig. 1 as a function of the flux density at 43 GHz. Since its accuracy depends on the value of the measured flux densities and associated uncertainties, we computed the expected 1σ as a function of the flux density, assuming a typical rms, associated with the 43 GHz and 5 GHz measurements, of $\sigma_{43\ \rm GHz} \approx 50$ mJy and a $\sigma_{5\ \rm GHz} \approx 35$ mJy, respectively. The $\pm 1\sigma$ uncertainty values around the mean value $\alpha = -0.09$ are shown in Fig. 1 as dot-dashed lines. For about 70% of the sources we obtain a spectral index inside the uncertainty lines, showing that it is statistically consistent with the value $\alpha = -0.1$, typical of an optically thin free-free emission. We conclude that for our sample, at least up to 43 GHz, the SED is dominated by the free-free emission and other contributions, if present, are negligible.

3.2. The dust contribution

PNs are usually surrounded by a dusty envelope which is the remnant of the precursor's wind. Dust thermally re-radiates the UV radiation of the central star determining an excess that may extend from the far-IR to the radio region. Such a contribution is typically of the order of 40% of the total flux from a PNe (Zhang & Kwok 1991), being larger in young PNe, since, in more evolved PNe, the circumstellar material has already dispersed. We built the dust component of our sample of PNe by using IRAS measurements.

The IRAS data have been fitted by assuming that the dust emits as a blackbody modified by the frequency dependent dust opacity, that is $F_\nu \propto \nu^p B_\nu(T_{\rm d})$, where $B_\nu(T_{\rm d})$ is the Planck function for the dust temperature $T_{\rm d}$, and p is the emissivity index. The index p strongly depends on the mineralogical composition of the grain and on their physical shape. In our calculation, following the results from detailed modelling of dust emission from PNe (Hoare 1990), we assumed, for the slope of the far-IR emissivity law, a typical value of $p = 1.5$. Because of the strong contamination by line emission of the 12 μm IRAS band (Stasinska & Szczerba 1999) only 25, 60 and 100 μm fluxes have been used in the fitting procedure, using only fluxes with a quality code better than 1.

4. Estimates of flux density in Planck channels

The SEDs with both ionized gas and the dust contribution, evaluated in Sects. 3.1 and 3.2, were built for all the targets in our sample. In Fig. 2, four such SEDs are shown as an example. In the SEDs, between the radio and far-IR there is a large gap where measurements are missing. New millimetre and sub-millimetre observations are clearly necessary to better characterize and constrain the emission from different components, where the radio flux, from the ionized fraction of the nebula, could be merged with the dust contribution. This gap will be partially filled by the ESA-PLANCK mission, as the satellite is equipped with a Low Frequency Instrument (LFI), operating at 30, 44 and 70 GHz, and a High Frequency Instrument (HFI), operating at 100, 143, 217, 353, 545 and 857 GHz.

In order to evaluate the possibility that PLANCK will actually detect sources in our sample, we should compare, for each observational band, the expected flux from the sources to the foreseen sensitivity. The expected fluxes are derived by summing, in each PLANCK channel, both the dust and ionized gas contribution. The first has been obtained by extrapolating the modified blackbody fit (dashed lines in Fig. 2); the latter has been obtained from fitting free-free emission from an optically thin nebula to the 5 GHz (6×10^4 μm) and 43 GHz (7×10^3 μm) data points and then extrapolating to the Planck channels (dotted line in Fig. 2), the NVSS measurements at 1.4 GHz (2×10^5 μm) have been also displayed.

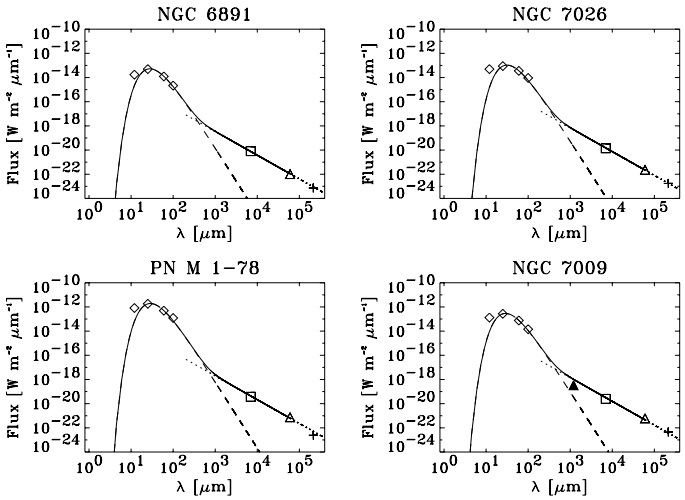

Fig. 2. Spectral Energy Distributions of four of our targets. Both ionized gas (dotted line) and thermal dust (dashed line) contributions are shown. The continuous line is the total emission. Diamonds: IRAS data; squares: our measurements at 43 GHz (7×10^3 μm); triangle: literature measures at 5 GHz (6×10^4 μm); cross: NVSS data at 1.4 GHz (2×10^5 μm); filled triangle: 250 GHz datum from Casassus et al. (2007).

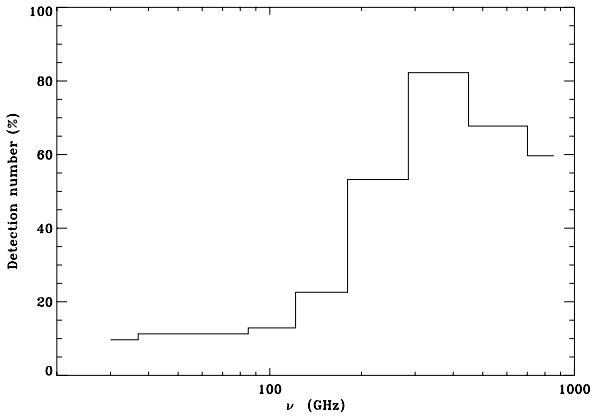

Fig. 3. Histogram showing the fraction of planetary nebulae belonging to our sample that can be detected by the Planck satellite.

Following Umana et al. (2006), the foreseen total sensitivity is assumed to be the sum in quadrature of all the sources of confusion noise, namely the nominal instrumental Planck sensitivity per resolution element, the Galactic and extragalactic foregrounds confusion noise (Toffolatti et al. 1998), the CMB confusion noise (Bennett et al. 2003). All the considered confusion sources will contribute to a total sensitivity (σ) ranging from 270 mJy for the 30 GHz channel to 220 mJy for the 857 GHz channel. In Fig. 3 we show the percentage of the objects from our sample that could be detected over the 3σ threshold for each channel of the PLANCK instruments. A small number of PNe belonging to our sample will be detected by PLANCK in the radio (LFI channels), while most of our targets will be easily seen by PLANCK in the millimetre and sub-millimetre bands (HFI channels).

Recently 17 sources in our sample were observed by Casassus et al. (2007) at 250 and/or 31 GHz. While the results of the measurements at 31 GHz (15 sources) agree quite well with our estimates, the 250 GHz measured fluxes (10 sources) appeared to be systematically lower, on average by a factor of 2, than our free-free extrapolations (see the SED of NGC 7009 in Fig. 2 as an example). Understanding whether the differences between our estimates and the Casassus et al. (2007) measurements are due to the sources being partially resolved at that frequency or to some intrinsic properties of the source, is beyond the scope of this paper. Casassus et al. (2007) claim that such an unexpected drop in the measured flux densities could be attributed to a synchrotron component absorbed by a cold nebular screen, but they also speculate about other possible emission/absorption mechanisms which may operate in the ionized part of the nebula, without reaching any firm conclusions. If we conservatively assume that such a peculiarity is present in all the PNe of our sample, the flux estimates in the 217 GHz PLANCK band has to be reduced by a factor of 2 and the expected detection rate in the same band reduces to about 20%. The estimates in the higher frequency bands remain unaffected due to the predominance of the thermal dust emission. We foresee an important contribution of the PLANCK mission also to the study of PNe, as it would provide measurements in a very important, but still poorly explored, spectral region.

5. Summary

We have presented new 7 mm (43 GHz) observations of a sample of radio-bright PNe, carried out with the INAF-IRA Noto Radiotelescope. Such observations have been used to derive the high-frequency free-free contribution, due to the ionized fraction of the circumstellar envelope. So far, the majority of high frequency radio observations of PNe have been conducted with interferometers, that reveal details of source radio morphology but could, in principle, resolve out some of the extended emission. Our single dish measurements provide an extended database of millimetre observations of PNe to be used when is necessary to know the overall emission such as when building a SED. We used our measurements that trace the free-free contribution together with IRAS measurements, which trace the thermal dust emission, to build up the observed SED from radio to far-IR and by extrapolation to estimate the expected fluxes in the spectral range between radio and sub-mm, where observational data are missing.

When comparing the expected millimetre-sub-millimetre fluxes with the total foreseen sensitivity of the forthcoming ESA PLANCK mission we estimate that a consistent number of our targets will be easily detected by PLANCK, mostly at higher frequency channels. Therefore, even if designed for cosmological study, PLANCK could also contribute to PNe investigation. Results from such kinds of observations, once modelled with the appropriate code (i.e. CLOUDY), would provide important constraints on the chemical composition and structure of the CSEs. The analysis of the modelled SEDs could point out the presence of multi-shells, related to multiple mass-loss event of the central object during its previous evolution (AGB), or a contribution of different emission processes, besides free-free and thermal emission from dust, as recently claimed by Casassus et al. (2007). Moreover, PLANCK results can be considered as pathfinders for future instrumentation, with the same frequency coverage, such as ALMA, as they will help in planning more focused experiments aimed to investigate the morphological details of the sources.

Acknowledgements. Based on obervations with the Noto Telescope operated by INAF-Istituto di Radioastronomia This work has been partially supported by ASI through contract Planck LFI Activity of Phase E2.

References

Acker, A., Ochsenbein, F., Stenholm, B., et al. 1992, ESOPN, 1, 1
Becker, R. H., White, R. L., & Edwards, A. L. 1991, ApJS, 75, 1
Bennett, C. L. 2003, ApJS, 148, 1
Casassus, S., Nyman, L. A., Dickinson, C., & Pearson, T. J. 2007, MNRAS, accepted [arXiv:0708.2385]
Condon, J. J., & Kaplan, D. L. 1998, ApJS, 117, 361
Condon, J. J., Kaplan, D. L., & Terzian, Y. 1999, ApJS, 123, 219
Gee, G., Emerson, J. P., Ade, P. A. R., Robson, E. I., & Nolt, I. G. 1984, MNRAS, 208, 517
Gomez, Y., Moran, J. M., Rodriguez, L. F., & Gray, G. 1989, ApJ, 345, 862
Gregory, P. C., Scott, W. K., Douglas, K., & Condon, J. J. 1996, ApJS, 103, 427
Griffith, M. R., Wright, A. E., Burke, B. F., & Ekers, R. D. 1994, ApJS, 90, 179
Griffith, M. R., Wright, A. E., Burke, B. F., & Ekers, R. D. 1995, ApJS, 97, 347
Haynes, R. F., Caswell, J. L., & Simons, L. W. J. 1979, AuJPA, 48, 1
Hoare, M. G. 1990, MNRAS, 244, 193
Hoare, M. G., Roche, P. F., & Clegg, R. E. S. 1992, MNRAS, 258, 257
Leto, P., Buemi, C. S., Trigilio, C., et al. 2006, MSAIS, 10, 87
Luo, S. G., Condon, J. J., & Yin, Q. F. 2005, ApJS, 159, 282
Kemper, F., Molster, F. J., Jager, C., & Waters, L. B. F. M. 2002, A&A, 394, 679
Milne, D. K. 1979, A&AS, 36, 227
Milne, D. K., & Aller, L. H. 1975, A&A, 38, 183
Ott, M., Witzel, A., Quirrenbach, A., et al. 1994, A&A, 284, 331
Perley, R. A., Zijlstra, A., & van Hoof, P. 2006, A&AS, 209, 9202
Siodmiak, N., & Tylenda, R. 2001, A&A, 373, 1032
Stasinska, G., & Szczerba, R. 1999, A&A, 352, 297
Tylenda, R., Siodmiak, N., Gorny, S. K., Corradi, R. L. M., & Schwarz, H. E. 2003, A&A, 405, 627
Toffolatti, L., Argueso Gomez, F., de Zotti, G., et al. 1998, MNRAS, 297, 117
Umana, G., Burigana, C., & Trigilio, C. 2006, MSAIS, 9, 279
van Hoof, P. A. M. 2000, MNRAS, 314, 99
Wright, A. E., Griffith, M. R., Burke, B. F., & Ekers, R. D. 1994, ApJS, 91, 111
Zhang, C. Y., & Kwok, S. 1991, A&A, 250, 179